SPRAY PYROLYSIS DEPOSITION FOR GAS SENSOR INTEGRATION IN THE BACKEND OF STANDARD CMOS PROCESSES

*Lado Filipovic and Siegfried Selberherr**

Institute for Microelectronics, TU Wien, Gußhausstraße 27-29/E360, A-1040 Wien, Austria

* Corresponding Author's Email: selberherr@iue.tuwien.ac.at

ABSTRACT

Gas sensors are based on metal oxides, which likely will have a considerable impact on future smart phones, are analyzed by means of simulations. The deposition of a thin tin oxide film at the backend of a CMOS process has enabled the manufacture of integrated gas sensors. A spray pyrolysis technique is implemented for the deposition step, resulting in a thin tin oxide layer with good step coverage and uniformity. A simulation approach for spray pyrolysis deposition is presented, along with a discussion of the gas sensor operation. A sample model for H_2 detection is suggested, while our research serves as a step to link the simulation of gas-sensitive material deposition and gas sensor operation.

INTRODUCTION

The integration of gas sensors in smart phones and wrist watches will revolutionize the way in which pollutants and harmful chemicals are detected in our environment. In Table I several target gases and the applications of their detection are listed [1].

TABLE I. APPLICATIONS FOR VARIOUS TARGET GASES

Application	Target gas
Fire/smoke detection	CO, H_2, NO_2
Indoor air quality	O_2, CO_2, VOCs
Pollution	CO_2, NO_x, O_3
Exhaust emission	H_xC_x, CO, NO_x, SO_2
Process monitors	NH_3, H_xC_x, SO_2
Breath analysis	VOCs
Toxic gas detection	CO, SO_2, H_2S

Until recently, available gas sensors relied on a bulky architecture and their manufacture was incompatible to that of conventional CMOS process sequences. CMOS integration is essential for combining the sensor with microelectronics. Metal oxide gas sensors rely on changes in its electrical conductance due to its interaction with a surrounding gas. They have been extensively studied in the hopes that they will provide the full gas sensing functionality with CMOS integrateability [2], [3], [4]. Tin oxide (SnO_2) has shown itself to be a powerful gas sensing material [2] while others such as zinc oxide [3], indium tin oxide, CdO, $ZnSnO_4$, NiO, etc, have also been widely researched [5]. The sensing principle of SnO_2 involves heating the layer locally to 150-400°C, while electrodes connect it to the CMOS circuitry, as depicted in Fig. 1.
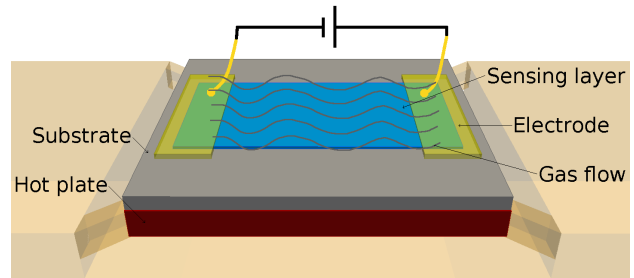

Fig. 1: Principle view of the gas sensor on a micro hot plate which is heated up to 150-400°C during operation.

The deposition of SnO_2 is performed using various techniques such as CVD [6], sputtering [7], pulsed-laser [8], sol-gel [9], and spray pyrolysis [10]. The spray pyrolysis technique has gained traction over its alternatives due to its cost effectiveness and ease of integration in the backend of a standard CMOS process. During the deposition process, a gas pressure nozzle is employed to atomize a $SnCl_4+H_2O$ solution. The nozzle is used to generate very small droplets which are directed towards the substrate, where SnO_2 is deposited, as shown in Fig. 2. With this method, substrates with complex geometries can be coated using CMOS-compatible temperatures below 400°C. The nozzle is placed about 30cm away from the substrate, ensuring that the droplets do not have a horizontal velocity when reaching the vicinity of the substrate.
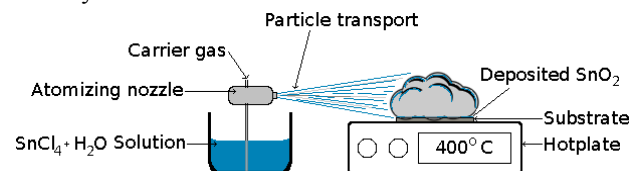

Fig. 2: Schematic of the experimental spray pyrolysis deposition process as set up for SnO_2 deposition.

SPRAY PYROLYSIS DEPOSITION

The steps which describe the processes taking place during spray pyrolysis deposition are: atomization of the precursor solution, aerosol transport of the droplet, and decomposition of the precursor to initiate film growth [11]. In this section, the dependence of the deposition time and temperature on the film thickness is introduced and an empirical model for the growth of tin oxide films is described. In addition, the sensor architecture is presented and the model is implemented in order to generate a full sensor structure, useful for further studies.

Model for Spray Pyrolysis Deposition

Several factors influence the film growth process, such as the distance between the nozzle and substrate, the length of the precursor solution aging, the air pressure, the solution volume, the temperature, and the deposition time [12]. For the presented model, the ambient pressure, the nozzle distance to substrate, and the solution aging remain constant. In Fig. 3, the deposited thickness' dependence on the deposition time is shown, when the temperature is set to 400°C. A linear relationship is evident, while a logarithmic dependence on the wafer temperature has also been observed [11]. An Arrhenius expression which best describes the deposition time (t, in seconds) and temperature (T, in Kelvin) dependence on the SnO$_2$ thickness (d, in μm) is given by

$$d(t,T) = A t \, e^{-E/k_B T}, \quad (1)$$

where A1=3.1μm/s and E=0.427eV. A 50nm thickness is reached after spray pyrolysis is performed for a 30 second burst at 400°C. The inlet of Fig. 3 suggests that, depending on the solution aging, a 31nm to 68nm thickness is to be expected [12]. With a half-day aged solution, a 50nm thickness is obtained under the same process conditions. When the technique is used to deposit a thin film on a step structure, no significant variation in the film thickness is noted [13]. This fact, combined with the high uniformity of the deposited film, means that the deposition occurs after the droplet approaches the heated substrate and forms a vapor. The droplets do not appear to impact the substrate surface in liquid form.
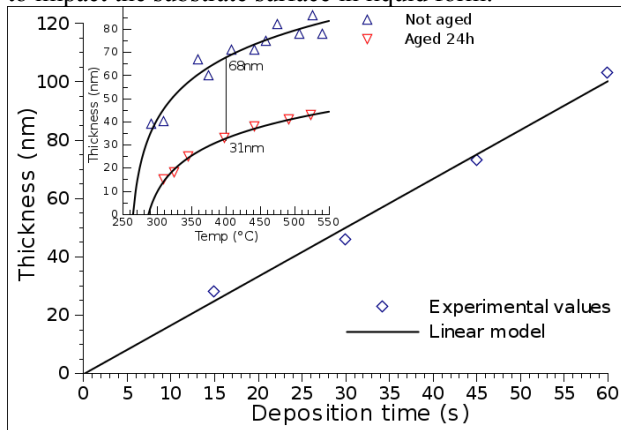
Fig. 3: Deposited SnO2 thickness versus deposition time. The inlet shows the dependence of temperature and solution aging on the deposited thickness. A half-day aged solution is used in the given experiment.

Spray Pyrolysis Deposition on Gas Sensor Geometries

The sensing layer of a gas sensor is deposited on top of a substrate which is provided with four electrodes, as shown in Fig. 4. The full structure is placed on top of an electrical insulating layer which separates the substrate from a heater placed below it.
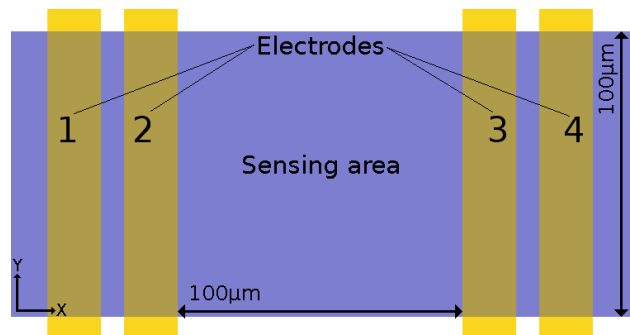
Fig. 4: Top view of the electrode locations on the substrate. The sensing area (SnO2) is deposited on top of the electrodes. The sensing area is 100μm x 100μm.

A two-dimensional view of a cut through the sensor geometry which includes the electrode metals and passivation layer is shown in Fig. 5. The tin oxide is deposited on the trench and step structure using the model given in (1). The simulation of the deposition on complex geometries is performed using a Monte Carlo method within a Level Set framework [14]. A single particle species is considered during the deposition. As the simulation is initiated, multiple particles are generated with a flux in the direction of the substrate. Each particle is described by its arriving direction and energy as well as its reflected direction and energy, should the particle not stick to its initial point of contact. It was found that a sticking coefficient of 0.01 has the best fit to experimentally-observed data and is therefore implemented in the model. Fig. 5 shows the resulting structure when a spray pyrolysis deposition is simulated at 400°C for 30 seconds. A 50nm SnO$_2$ film covers the passivation and electrode layers.
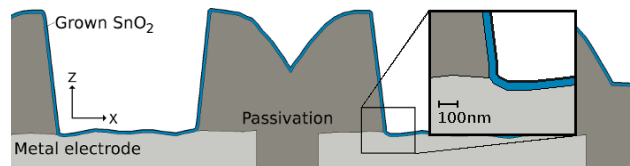
Fig. 5: Geometry of the deposited SnO2 on the Aluminum electrodes and silicon oxide passivation.

TIN OXIDE SENSOR ANALYSIS

The resulting simulated structure is imported into a finite element tool in order to determine the resistivity and stress distribution in the sensor structure.

Determining Tin Oxide Resistivity

The material parameters used during the simulation are given in Table II. The resistance of the full structure, between electrode 1 and electrode 4 from Fig. 4, is measured to be approximately 10.7kΩ. This corresponds to a resistivity of about 0.05Ω·cm, which is in the general range of values given in [17]. There is, however, a strong

dependence on temperature for the SnO2 V-I curve and thereby also on the gas sensor resistance, as shown in Fig. 6. The reason for this temperature dependence has to do with the adsorption of oxygen on the SnO2 surface, leading to band bending, described in the next section. The resistance in Fig. 6 is measured using a 4-point configuration, including all four aluminum electrodes [18]. When the device is operating at temperatures above 300°C the resistance remains at approximately 30kΩ.

TABLE II.   PROPERTIES OF TIN OXIDE

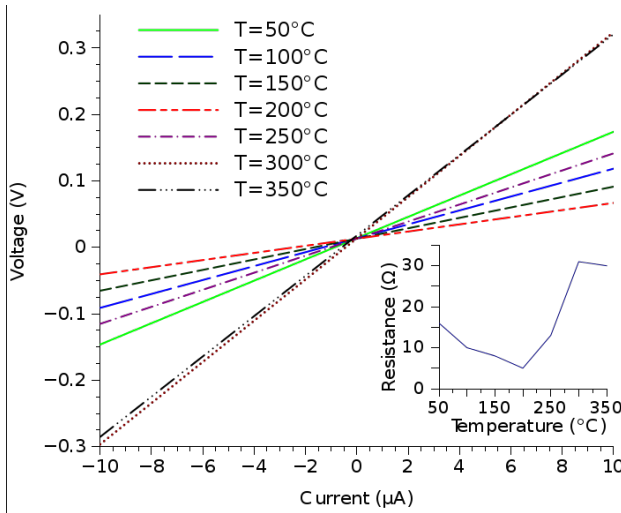| SnO2 parameter	Value		Ref.
Density	6.95	g·cm^{-3}	[15]
Resistivity (T$_{room}$)	5·10^{-2}	Ω·cm	[17]
Thermal conductivity	0.4	W·cm^{-1}·K^{-1}	[16]
CTE	4·10^{-6}	K^{-1}	[15]

Fig. 6: V-I curve dependence on operation temperature.

Thermo-Mechanical Stress in Tin Oxide Gas Sensors

After the spray pyrolysis deposition and annealing steps are performed at 400°C, the structure is cooled to room temperature. In addition, the operation of the gas sensor requires constant heating of the gas sensing layer to temperatures between 150°C and 400°C. This temperature variation can cause stresses between the passivation, aluminum electrodes, and tin oxide layers due to their different coefficients of thermal expansion (CTE). Fig. 7 shows the stress distribution through the section of the sensor where the electrodes, SiO2 and SnO2 are present. The highest stress appears in the SiO2 layer between the two aluminum electrodes. This is not surprising, because the aluminum tries to expand the most due to a high CTE of 23·10^{-6}K^{-1}, while the oxide expands the least, with a CTE of 0.5·10^{-6}K^{-1}. The maximum and average stresses through the SnO2 layer are found to be 800MPa and 200MPa, respectively.
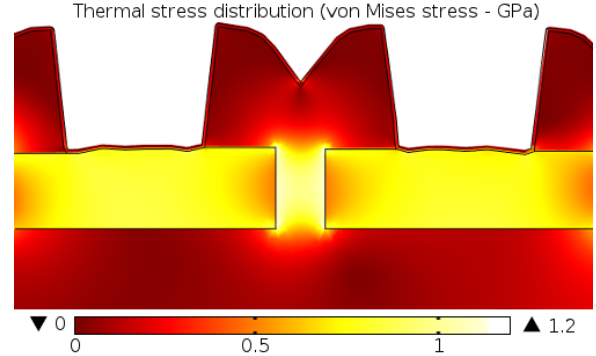

Fig. 7: Thermal stress distribution (von Mises) through the tin oxide, passivation, and aluminum electrode layers after cooling the chip to room temperature from 400°C.

TIN OXIDE SENSOR OPERATION

A simple explanation for the operation of metal oxide gas sensors is that at temperatures between 150°C and 400°C oxygen is adsorbed at the metal oxide surface by trapping electrons from the bulk. The result is an overall resistance decrease or increase for an n-type or p-type material, respectively, depicted with band bending at the metal oxide/air interface in Fig. 8. The introduction of a target gas in the atmosphere causes a reaction with the oxygen species, removing them from the interface and reducing the band bending effect and thereby the overall resistance [19].
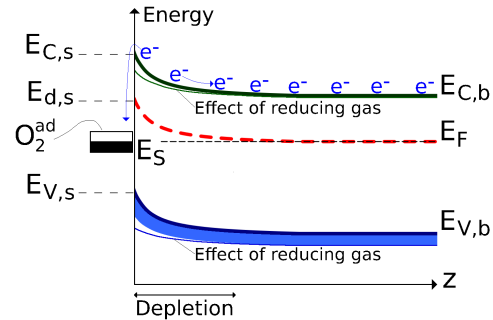

Fig. 8: Schematic representation of the band bending effect caused by oxygen adsorption and subsequent introduction of a reducing gas.

The thickness of the depletion layer is in the order of the Debye length, defined by

$$\lambda_D = \frac{\sqrt{\varepsilon_0 k_B T}}{q^2 n_C}, \quad (2)$$

where ε_0 is the free space permittivity, q is the elementary charge and n_C the carrier charge density. The structure of the sensing layer will influence the sensing process. When a porous layer is deposited, the gas species can penetrate into the tin oxide to react at the surface of the grains and grain boundaries [20], as shown in Fig. 9.
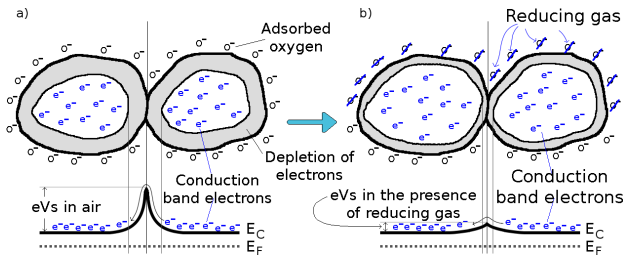
Fig. 9: Gas sensing function and conduction mechanism for a porous metal oxide, where the oxygen and reducing gas can penetrate to interact with each grain.

However, for compact SnO_2 films, such as the one presented here, the oxygen adsorption and reaction with a reducing gas only occurs at the surface [19], as depicted in Fig. 10.
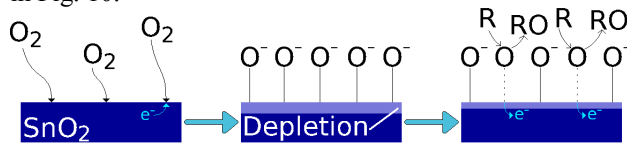

Fig. 10: Gas sensing function for a compact tin oxide film. The reaction occurs only at the top surface of the deposited tin oxide. Symbol R refers to a reducing gas.

Model for the Detection of Atmospheric H_2

Two sensor structures have been used in order to test the sensor's response in the presence of H_2 at a 350°C temperature [18]. The dimensions of the two structures are 100μm x 100μm and 100μm x 5μm. A 50nm layer of SnO_2 has been deposited using spray pyrolysis, as described in the previous sections. The effect of the presence of H_2 in the atmosphere on the normalized resistance and the equations which represent the relationship are shown in Fig. 11. The relationship can be represented as

$$R_{norm} = R_0 - m \ln(H_2), \quad (3)$$

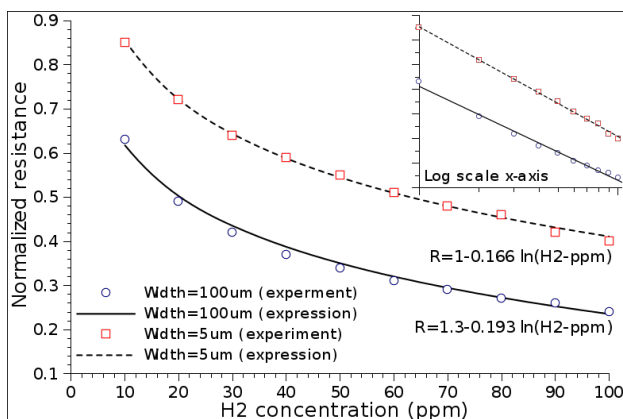where R_0 and m are geometry-dependent variables and H_2 is given in ppm.

Fig. 11: Normalized resistance dependence on H_2. A logarithmic relationship is evident.

CONCLUSION

Tin oxide based gas sensors have been analyzed through simulations and a Level Set based simulation approach for the spray pyrolysis deposition of SnO_2 on complex geometries has been presented. The resistivity and stress of the generated structure was analyzed using finite element simulations, showing that using aluminum as an electrode material may lead to high stress in the passivation layer. An initial approach to model the device operation has also been discussed and a logarithmic dependence on H_2 for the material resistivity is observed.

REFERENCES

[1] E. Brunet, Fabrication of Tin Oxide Nanowire Gas Sensors, Dissertation, Technische Universität Wien, Fakultät für Technische Chemie (2014).

[2] G. Korotcenkov, *Mater. Sci. Eng. B*, vol. 139, no. 1, pp. 1-23, 2007.

[3] M. Ortel et al., *Solid-State Electron.*, vol. 86, pp. 22-26, 2013.

[4] J. W. Gardner et al., *IEEE Sens. J.*, vol. 10, no. 12, pp. 1833-1848, 2010.

[5] A. Bouaud et al., *Mater. Chem. Phys.*, vol 137, no. 3, pp. 843-847, 2013.

[6] I. Volintiru et al., *Thin Solid Films*, vol. 519, no. 19, pp. 6258-6263, 2011.

[7] J. Boltz et al., *Surf. Coat. Technol.*, vol. 205, no. 7, pp. 2455-2460, 2010.

[8] S. Sinha et al., *Mater. Lett.*, vol. 65, no. 2, pp. 146-149, 2011.

[9] D. M. Cavatho et al., *J. Sol-Gel Sci. Technol.*, vol. 55, no. 3, pp. 385-393, 2010.

[10] G. Patil et al., *ISRN Technol.*, vol. 2012, p. 275872 (1-5), 2012.

[11] D. Perednis and L. J. Gauckler, *Solid State Ion.*, vol. 166, no. 3-4, pp. 229-239, 2014.

[12] G. Korotcenkov et al., *Sensor Actuators B*, vol. 77, no. 1-2, pp. 244-252, 2001.

[13] L. Filipovic et al., *IEEE Trans. Semiconduct. Manufact.*, vol. 27, no. 2, pp. 269-277, 2014.

[14] L. Filipovic et al., *Eng. Lett.*, vol. 21, no. 4, pp. 224-240, 2013.

[15] M. Batzill and U. Diebold, *Prog. Surf. Sci.*, vol. 79, no. 2, pp. 47-154, 2005.

[16] C. Poulier et al., *J. Eur. Ceram. Soc.*, vol. 27, no. 2, pp. 475-478, 2007.

[17] J. Joseph et al., *Turkish J. Phys.*, vol. 33, pp. 37-47, 2009.

[18] G. C. Mutinati et al., *Procedia Eng.*, vol. 47, pp. 490-493, 2012.

[19] N. Barsan and U. Weimar, *Proceedings of IMCS 2012*, Nuremberg, Germany, May 20-23, 2012, pp. 618-621.

[20] N. Barsan et al., *Sensor Actuator B*, vol. 121, no. 1, pp. 18-35, 2007.